Original Article

Enabling Histopathological Annotations on Immunofluorescent Images through Virtualization of Hematoxylin and Eosin

Amal Lahiani[1], Eldad Klaiman[1], Oliver Grimm[1]

[1]Roche Pharma Research and Early Development, Pathology and Tissue Analytics, Roche Innovation Center, Munich, Penzberg, Germany

Received: 21 September 2017 Accepted: 24 November 2017 Published: 14 February 2018

Abstract

Context: Medical diagnosis and clinical decisions rely heavily on the histopathological evaluation of tissue samples, especially in oncology. Historically, classical histopathology has been the gold standard for tissue evaluation and assessment by pathologists. The most widely and commonly used dyes in histopathology are hematoxylin and eosin (H&E) as most malignancies diagnosis is largely based on this protocol. H&E staining has been used for more than a century to identify tissue characteristics and structures morphologies that are needed for tumor diagnosis. In many cases, as tissue is scarce in clinical studies, fluorescence imaging is necessary to allow staining of the same specimen with multiple biomarkers simultaneously. Since fluorescence imaging is a relatively new technology in the pathology landscape, histopathologists are not used to or trained in annotating or interpreting these images. **Aims, Settings and Design:** To allow pathologists to annotate these images without the need for additional training, we designed an algorithm for the conversion of fluorescence images to brightfield H&E images. **Subjects and Methods:** In this algorithm, we use fluorescent nuclei staining to reproduce the hematoxylin information and natural tissue autofluorescence to reproduce the eosin information avoiding the necessity to specifically stain the proteins or intracellular structures with an additional fluorescence stain. **Statistical Analysis Used:** Our method is based on optimizing a transform function from fluorescence to H&E images using least mean square optimization. **Results:** It results in high quality virtual H&E digital images that can easily and efficiently be analyzed by pathologists. We validated our results with pathologists by making them annotate tumor in real and virtual H&E whole slide images and we obtained promising results. **Conclusions:** Hence, we provide a solution that enables pathologists to assess tissue and annotate specific structures based on multiplexed fluorescence images.

Keywords: Brightfield images, classical histopathology, fluorescence images, histopathological evaluation, virtual hematoxylin and eosin

Introduction

Pathology is the study and diagnosis of diseases including cancers and has long been associated with medical development and patient care and treatment. More specifically in histology, samples of tissue are taken from patients and then prepared using appropriate staining protocols to detect and diagnose the disease. Hematoxylin and eosin (H&E) staining is the standard protocol used in histology as it gives a good overview of the tissue and the cellular components and it clearly shows different types of structures. It is very useful to assess the presence or absence of disease processes in the tissue and to measure disease progression. It is also likely that this protocol continues being used in the next decades.[1] Hematoxylin is a basic dye staining acidic components in shades of purple and blue and eosin is an acidic contrasting counterstain coloring the basic components (mostly proteins) in shades of pink and red.[2] In a normal H&E stain, cell nuclei are colored in blue and purple whereas cell cytoplasm and most connective tissue are colored in degrees of pink [Figure 1].

Major industry trends in pathology and tissue analytics include the adoption of tissue image digitization, automatic image analysis, and multiplexing of biomarkers as key steps for streamlining drug development and improving the quality of cancer diagnosis and care. H&E staining contains important visual information that allows assessing tissue morphology but is not compatible with

Access this article online

Quick Response Code:

Website: www.jpathinformatics.org

DOI: 10.4103/jpi.jpi_61_17

Address for correspondence: Ms. Amal Lahiani, Nonnenwald 2, 82377 Penzberg, Germany. E-mail: amal.lahiani@roche.com

How to cite this article: Lahiani A, Klaiman E, Grimm O. Enabling histopathological annotations on immunofluorescent images through virtualization of hematoxylin and eosin. J Pathol Inform 2018;9:1.

Available FREE in open access from: http://www.jpathinformatics.org/text.asp?2018/9/1/1/225491

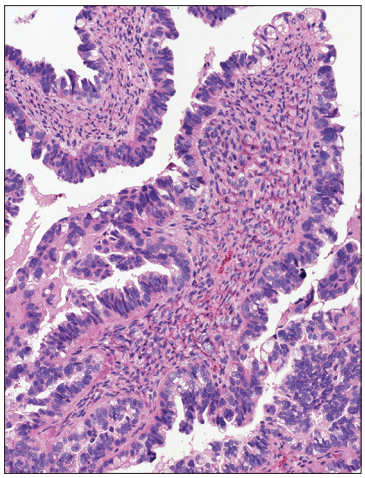

Figure 1: Field of view of a slide stained with typical hematoxylin and eosin. Cell nuclei are colored in shades of blue and purple and connective tissue is colored in shades of pink

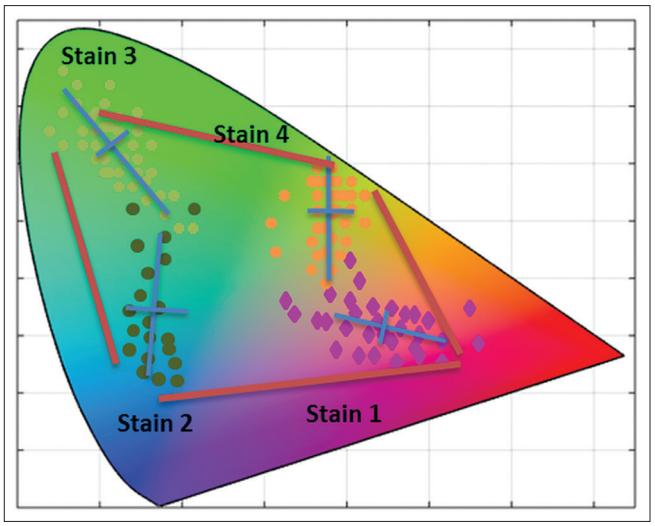

Figure 2: The color space created as a planar representation of the RGB optical density space. When imaging with an RGB scanner, hues inside the polygon spanned by the four reference stains are ambiguous, for example, there are multiple combinations of up to three stains that can result in this hue

multiplex biomarker staining technology. In general, brightfield microscopy staining is limited in the number of simultaneous different separable stains that can be made on a single section due to the nature of the color space. When slides are imaged with stains having overlapping spectra [Figure 2], color deconvolution might not provide an accurate result, leading to misdetection of biomarkers. This problem is further complicated when more than three biomarkers are present on the same slide.[3,4]

In contrast, with fluorescence staining and microscopy technology, multiple biomarkers can be stained and imaged in separate channels. This enables easy separation between biomarkers for automatic analysis algorithms, but pathologists are nowadays not able to examine or annotate tissue in fluorescence images [Figure 3].

One of the major challenges is to enable multiplexing of different biomarkers while retaining the advantages of H&E in terms of morphology information. However, the current fluorescent staining technology (e.g., tyramide signal amplification) does not yet allow simultaneous combination of H&E dyes and fluorescent dyes on the same slide due to the fluorescent characteristics of H&E and chemical interaction between them and the fluorescent antibodies.[5] Using consecutive sections to obtain brightfield and fluorescent images might be problematic when the amount of tissue is limited and might also introduce artifacts due to the difference that exists even between consecutive slides. Sequentially imaging one slide with H&E dyes then with fluorescent dyes requires a washing step between the two types of staining and introduces additional and sensitive laboratory work. All of these methods additionally require the registration of the two images obtained with the different modalities. In order to overcome these challenges, we developed an algorithm that transforms in real time the fluorescence images into H&E like images.

Several attempts have been made to generate virtual H&E images from other modalities in order to facilitate the interpretation of fluorescent images and allow pathologists to perform both quantitative analysis and pathologic diagnostics using the same set of fluorescent images. Reflectance and fluorescence confocal microscopy images were compared to standard classical H&E histology in the previous studies,[6-8] but these types of images show reduced stromal details in comparison with nuclear details. Reflectance and confocal images are also different from classical histopathological images; it is then necessary for pathologist to understand the correlation between these images and traditionally prepared slides. In another study, a false coloring technique using confocal reflectance and fluorescence images was used in order to mimic H&E histologic staining[9,10] and facilitate the interpretation and annotation of images by pathologists. Dobbs *et al*. developed a similar method using only confocal fluorescent images.[11]

In these three studies, virtual H&E images were obtained by adding the transmission spectra of the dyes which is physically not realistic.[12] A linear least square estimation was used in the study by Can *et al*.[13] to estimate the intensity transformation that maps the fluorescent images into the brightfield color space, but the assumption of a linear transformation between darkfield (fluorescent) and brightfield images is not necessarily realistic. Tao *et al*.[14] demonstrated that using nonlinear microscopy (NLM) and mapping the NLM-detected channels into virtual H&E colors allow to achieve results in 95.4% sensitivity and 93.3% specificity for the assessment of breast pathologies compared to paraffin-embedded H&E histology. Nevertheless, no clear algorithm for mapping NLM channels to virtual H&E was described.

Giacomelli *et al*.[12] demonstrated a physically realistic rendering approach modeling the transmission of a wavelength through a specific thickness of a specimen containing N

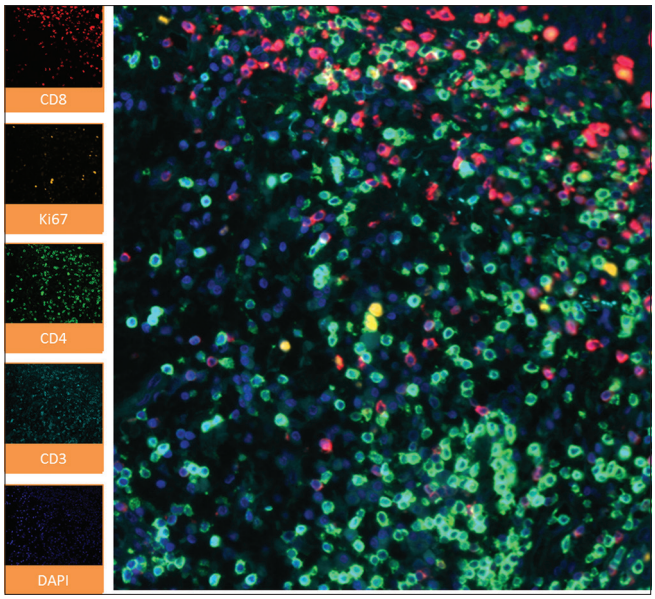

Figure 3: Field of view of a slide stained with an immunofluorescence assay targeting CD8 (Cy5 - red), Ki67 (Cy3 - yellow), CD4 (FITC - green), CD3 (CFP - light blue), and nuclei (DAPI - dark blue). All fluorescence channels are combined in an RGB darkfield image. This type of images is still difficult to examine or annotate by pathologists

absorbing dyes using a discrete model based on optical density from Beer–Lambert law.[15] Giacomelli *et al*. described the virtual H&E image in the RGB color space as:

$$M = Exp\left(-\beta_{HTX,M} c_{HTX} - \beta_{Eos,M} c_{Eos}\right) \quad (1)$$

In equation (1), HTX and Eos are abbreviations for H&E, respectively, M corresponds to one of the 3 RGB color channels, C_i corresponds to the concentration of the dye *i* and $\beta_{i,M}$ corresponds to the attenuation of the i^{th} dye integrated over the spectral range of the M^{th} color channel.

Assuming a linear relationship between the intensity emitted by a fluorophore and the concentration of a dye, the virtual H&E equations become then:

$$M = Exp\left(-\beta_{HTX,M} I_{DNA} k - \beta_{Eos,M} I_{Proteins} k\right) \quad (2)$$

Where *k* corresponds to a scaling factor accounting for the linearity between the intensity emitted by the fluorophore and the concentration of the dye and I_{DNA} and $I_{proteins}$ are the fluorescence signals corresponding to DNA and proteins, respectively. Giacomelli *et al*. used DAPI and eosin as the fluorescence signals corresponding to DNA and proteins, respectively. An arbitrary and unique scaling factor k was used for both H&E dyes and $\beta_{i,M}$ was obtained using the output color space (for instance sRGB). However, defining a standard color for a dye is highly subjective due to tissue, laboratory protocol, staining, scanner, and capture parameter variability.[16] In addition, the definition of an ideal H&E image depends on the pathologist and differs from person to person.

In order to combine the advantages of H&E morphology and multiple biomarker detection, we developed an algorithm to generate virtual H&E images from fluorescent images meeting the essential requirements for identifying morphological compartments in the tissue. For this purpose, we propose a general method for the determination of the parameters in equation (2) by means of minimizing an error function between the virtual H&E images and the real H&E staining of the same tissue samples. In real-life scenarios, tissue staining assays and imaging protocols are optimized for a specific goal, and fluorescent assays in particular are influenced by each additional dye used; hence, we want to avoid the need to add a protein staining, for example, eosin to our operational assays. Since the protein image information already exists in the fluorescence images in the form of autofluorescence,[17] we attempted to use this information for the reproduction of the eosin channel in the virtual H&E without the need for additional changes in the staining assays.

Subjects and Methods

Different human tissue sections were used. Specimen slices were cut at a thickness of 2.5 μM with a rotary microtome then dried for 20 min at 60°C. Tissue sections were firstly stained with the fluorescent dyes sequentially; a coverslip with Fluoro-Gel Mounting Medium with DAPI was used in the fluorescent staining; the sections were washed after each fluorescence staining in order to remove the inactivated antibodies. The slides were subsequently scanned with a Zeiss Axio Z1 microscope scanner. Then, the same sections were incubated in warm water (40°C) in order to remove coverslip and stained with H&E before being scanned in a Ventana iScan HT brightfield microscope scanner. In the H&E staining, a Ventana Symphony coverslip was used. This method allows us to have the same parts of tissue stained with both brightfield and fluorescence enabling us to perform a pixel-wise comparison between brightfield and fluorescence images.

The fluorescence scanning results in 5 layers of 16-bit intensity images, each intensity image corresponding to a biomarker. We labeled the specimens with the fluorophores Cy5, Cy3, FITC, CFP, and DAPI corresponding, respectively, to the biomarkers CD8, Ki67, CD4, CD3, and nuclei. CD3, CD4, and CD8 are protein complexes associated with T-cells, Ki67 is a nuclear marker for cell proliferation, and DAPI binds to DNA and corresponds to nuclei. The H&E scanning yields 24-bit RGB images with levels of purple and pink corresponding to H&E, respectively.

The fluorescence and brightfield images of the exact same tissue allow us, after image registration, to compare each pixel with the corresponding pixel in the other imaging modality. In turn, this comparison enables the optimization of the transform function parameters minimizing the mean square error between the virtual H&E and the real H&E. These optimized parameters will then have the advantage of having been systematically optimized for multiple and different tissue samples [Figure 4].

As we described in previous sections, our goal is to digitally generate virtual H&E images that could be used by pathologists

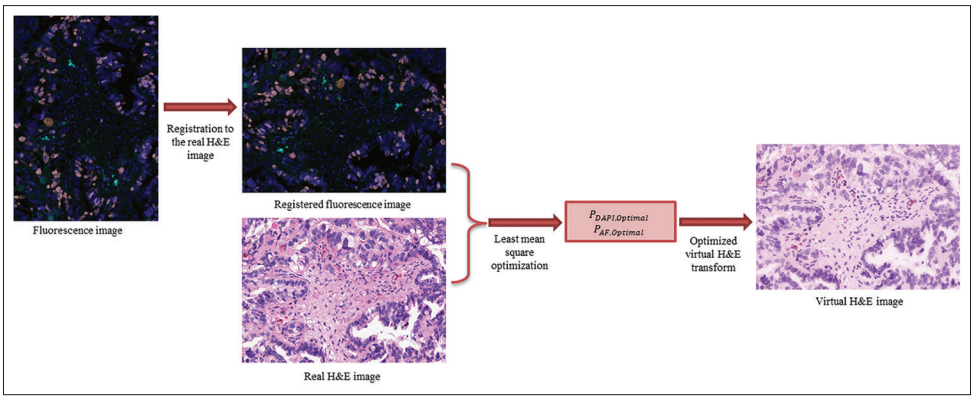

Figure 4: Simplified process of obtaining virtual hematoxylin and eosin images from fluorescence images. We used 5 field of views from different slides to get the optimized transform parameters. We performed manual registration by selecting control points then fine-tuning by manual rotations and shifts to the single pixel accuracy

for annotation and interpretation of tissue samples. For this, we start from the physical demonstration described by Giacomelli *et al*.[12] Since in Giacomelli *et al*.'s study, the parameters k and $\beta_{i,M}$ in equation (2) are selected heuristically and multiplied, we use a simplified version of this equation in which k and $\beta_{i,M}$ are combined into one parameter yielding:

$$M = Exp\left(-P_{DNA,M}\, I_{DNA} - P_{Proteins,M}\, I_{Proteins}\right) \quad (3)$$

Using equation (3), we associated the fluorescence signals of DNA and proteins to our fluorescence channels. As autofluorescence and eosin correspond to proteins in fluorescence and brightfield images, respectively, we associated the fluorescence signal of protein $I_{Proteins}$ to autofluorescence. Actually, autofluorescence corresponds to the natural emission of light by some parts of the tissue (mostly proteins). These proteins, when excited with a specific wavelength, pass to an excited state and then emit a fluorescent light resulting in a loss of energy and a return to the ground state.[17] In addition, as we explained above, hematoxylin and DAPI are both nuclear markers. That is why, we have chosen the corrected DAPI channel after removing the autofluorescence as the fluorescence signal for the DNA I_{DNA}. The virtual H&E equation becomes then:

$$M = Exp\left(-P_{DAPI,M}\, I_{DAPI} - P_{AF,M}\, I_{AF}\right) \quad (4)$$

Where AF is an abbreviation for autofluorescence.

As can be seen from equation (4), we have 6 parameters to optimize ($P_{DAPI,R}$, $P_{DAPI,G}$, $P_{DAPI,B}$, $P_{AF,R}$, $P_{AF,G}$, $P_{AF,B}$). Since the slides were stained with both H&E and fluorescence on the same tissue, we can, after slide registration, assume that pairs of corresponding pixels in these images exist. Applying equation (4) to the fluorescence pixels and comparing to the same pixel in the brightfield image enables us to derive a square error measure. We can then use a least mean square optimization technique to minimize the error and obtain the optimal parameters for the virtual H&E transformation.

We obtain the autofluorescence image from the fluorescence image by defining an autofluorescence spectral profile of relative intensities between the scanned fluorescence channels and by removing a multiple of this profile from the spectral profile of each fluorescence image pixel so that the remaining spectral profile of the pixel is as sparse as possible. We assume that a single pixel could have, biologically speaking, signal in only a limited number of channels[17] and that at least one of the channels in the spectral profile of each pixel should be zero. For example, in the fluorescence staining we used, it would be extremely improbable to have membrane (i.e., CD3/CD8) and nucleus (DAPI) staining in the same pixel. We calculate a factor which when multiplied by the autofluorescence spectral profile and removed from the pixel spectral profile yields at least one zero value channel in the pixel.

Registration of the fluorescence and the H&E images was done manually with a custom-made Matlab user interface (UI) in which we registered the images by selecting corresponding control points in the image pairs. The UI also allowed fine-tuning by manual rotations and shifts to the single pixel precision. Since the pixel sizes of the fluorescence and brightfield microscopes are 0.465 and 0.324, respectively, we set the scale parameter of the registration transform to a fixed value corresponding to the physical ratio between both pixel sizes.

Once the fluorescence and the H&E images are registered, we perform a least mean square optimization on the pairs of pixels in both images to optimize the parameters P_{DAPI} and P_{AF}. We used 5 pairs of registered fields of views (FOVs), sized 2048 × 2048 pixels, to perform the optimization. Using more FOVs in the optimization did not influence much either the optimized parameters or the resulting images. From equation (4), we can see that the logarithm of the virtual H&E images is a linear function of the fluorescence images I_{DAPI} and I_{AF}.

In the optical density space, the system could be written as:

$$\log(R) = -P_{DAPI,R}\, I_{DAPI} - P_{AF,R}\, I_{AF} \quad (5)$$

$$\log(G) = -P_{DAPI,G}\, I_{DAPI} - P_{AF,G}\, I_{AF} \quad (6)$$

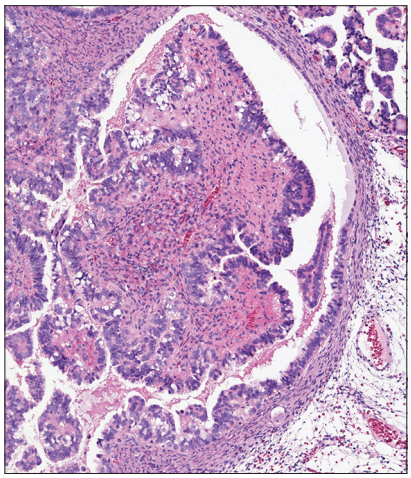

Figure 5: Real hematoxylin and eosin image stained with the classical process

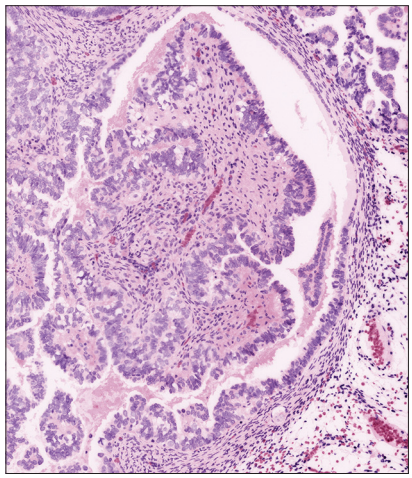

Figure 6: Virtual hematoxylin and eosin image obtained with the optimized parameters

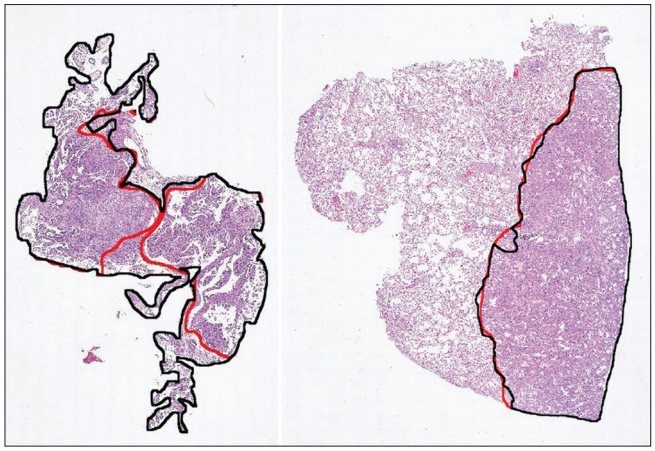

Figure 7: Results of tumor annotation done by pathologists on two examples of real hematoxylin and eosin images. The red and black lines correspond to tumor annotations done by the two pathologists, respectively

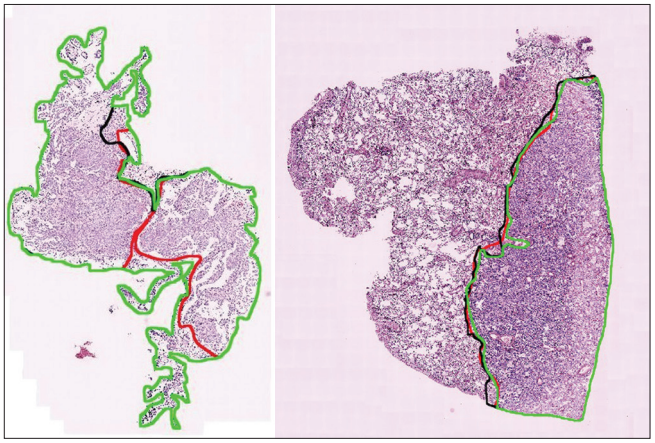

Figure 8: Results of tumor annotation done by pathologists on the corresponding virtual hematoxylin and eosin images. The red and black lines correspond to tumor annotations done by the two pathologists, respectively. The green line corresponds to the annotation made by the third pathologist on the virtual hematoxylin and eosin image

$$\log(B) = -P_{DAPI,B} I_{DAPI} - P_{AF,B} I_{AF} \quad (7)$$

Where R, G, and B correspond to the three RGB channels.

Using a matrix representation, we get the following equation:

$$\log(M) = IP(M) \quad (8)$$

M is a column vector of a specific color channel in the H&E image, P is a column vector of P parameters for the channel M transform, and I is a two-column matrix consisting of the DAPI and AF fluorescence channels.

After optimization, we apply the virtual H&E transform (equation [4]) with the optimized parameters to a set of fluorescence images for which we have also the real H&E staining in order to check the performance of our algorithm.

In the next step, we evaluated our results subjectively by having them annotated by pathologists for tumor and compared to the tumor annotations made by pathologists on the real H&E images. For this purpose, we used 5 couples of real/virtual H&E whole slide images. We quantify the similarity between annotations by using the Dice coefficient.[18]

Considering two samples A and B, Dice coefficient could be written as:

$$D = \frac{2|A \cap B|}{|A| + |B|} \quad (9)$$

In our case, A and B are, for instance, tumor annotations done by a pathologist on real and virtual H&E images, respectively.

Results

Following least mean square optimization using a training set that consisted of 5 FOVs (corresponding to 20971520

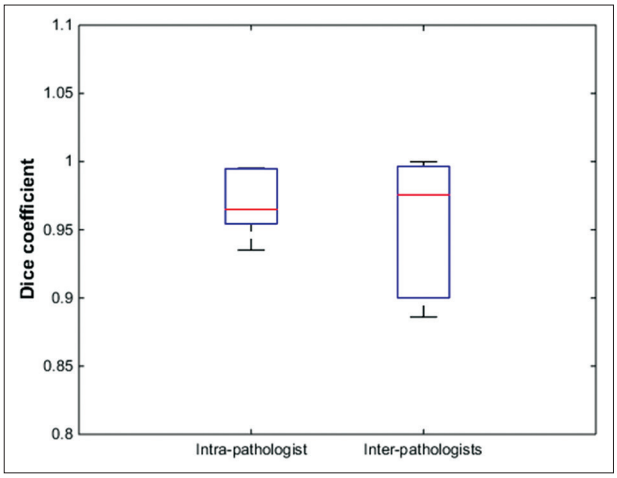

Figure 9: Boxplot representation of Dice coefficients of the pairs of slides (real/virtual hematoxylin and eosin) annotated by the same pathologists (intrapathologist) and by different pathologists (interpathologists). The central mark (red line) corresponds to the median, the edges of the box correspond to the 25th and 75th percentiles, and the whiskers extend to the minimum and maximum values. The average Dice coefficient intrapathologist is equal to 0.97 and the average Dice coefficient interpathologists is equal to 0.95

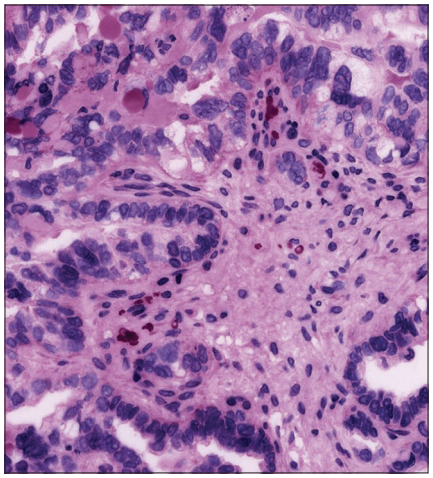

Figure 11: The corresponding virtual hematoxylin and eosin field of view. The structures are similar in the real and virtual hematoxylin and eosin images

pixels) from different slides, we applied the optimized H&E transform to whole slide images. We performed a comparison between the virtual H&E images and the corresponding real H&E images [e.g., Figures 5 and 6] based on pathologists' evaluation. From Figures 5 and 6, we can visually see that the real and virtual H&E images are quite similar and show the same details both microscopically and macroscopically.

Pathologists' annotations on slide images consist of defining areas with specific characteristics and are used as regions of interest for the automatic analysis algorithms and data exploration. Since in our case, the aim of this virtualization of H&E is to enable pathologists to annotate tumor on fluorescent-stained images, it seemed natural to choose the

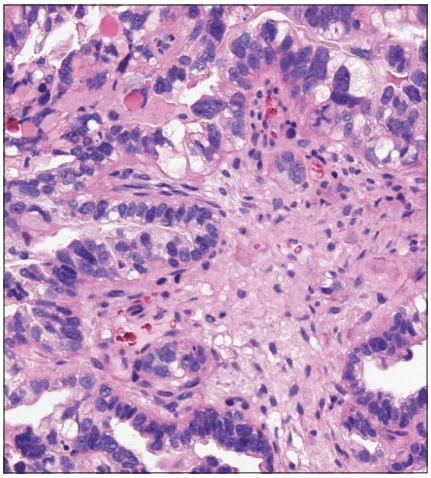

Figure 10: Real hematoxylin and eosin field of view

similarity of these annotations on both real and virtual H&E images as a measure for the quality of the virtualization transform. This method was also used in previous brightfield virtualization studies[11] and presents a very practical and functional measure of the quality of the transformation, allowing us valuable insight into the question of "if" and "how" the virtualization of brightfield-stained images affects the underlying visual data and patterns used by the pathologists to diagnose and identify anomalies in the tissue. A disadvantage of this case pointed out to us by our expert pathologist team is that because they see both the real and virtual images they might tend to annotate both the same way even if some time elapses between annotations since they have a developed "photographic" memory when it comes to tissue sections. We address this problem by comparing annotations made only on virtual H&E images by one pathologist to the annotations made on real H&E images by another pathologist. Since neither of them saw the others annotations, the comparison can give insight into the actual difference between real and virtual H&E annotation without bias. Five tissue samples containing tumor were stained with our fluorescence assay, imaged, and converted to virtual H&E. The slides were then washed and restained with H&E and imaged again in a brightfield scanner. Two pathologists annotated the pairs of real and the virtual H&E images, and one pathologist annotated only virtual H&E images. We used Dice coefficient to evaluate the similarity between the annotations. The intrapathologist Dice coefficient measures the similarity between the annotations made by the same pathologist on the real and the virtual H&E images. The interpathologist Dice coefficient measures the similarity between the annotations made by the third pathologist annotating only on the virtual H&E images and the annotations made by the other pathologists on the real H&E images. High intrapathologist Dice coefficients mean that a pathologist annotated the real and virtual images very similarly. High interpathologists Dice coefficients mean that the pathologist annotating the virtual image only, annotated it very similarly to how the other pathologists annotated the real

image. This also mitigates the potential bias from pathologist visual memory when annotating both virtual and real images.

Figures 7 and 8 show two examples of tumor annotation results done by pathologists on the real and the virtual H&E slides.

We computed the Dice coefficient on the set of real and virtual H&E slide pairs annotated by pathologists [Figure 9]. The average Dice coefficients intrapathologists and interpathologists are equal to 0.97 and 0.95, respectively. Both values are close to 1.0 which reflects a good match between the pathologist tumor annotations made on virtual compared to annotations made on real images. The number of slides in the validation set does not allow a statistical comparison between the values of the interpathologist and intrapathologist Dice coefficients.

Discussion

The objective of this work is to generate virtual H&E images using fluorescence images to enable medical diagnosis and to combine the advantages of fluorescence multiplexing and brightfield image familiarity and ease of annotation. Fluorescent staining allows the staining of several different biomarkers within the same specimen but creates multilayered image which is not trivial for a pathologist to annotate. Pathologists are very familiar with classical histopathology and specifically H&E staining which has been the standard staining used for tissue diagnosis for over a century. In addition, fluorescence staining and imaging technologies are relatively new and are still not the standard methods used in the clinic. This conflict lies at the core of the motivation for this study since we wish to use fluorescence imaging in the context of cancer drug research and development, but we rely on pathologists to annotate and diagnose tissue as part of this process. We aim to virtually reproduce classical histopathology images in high-quality virtual H&E images to empower pathologists in the diagnosis and annotation of complex fluorescence scenes.

Our approach aims to solve the gap presented by the lack of eosin stain in our staining assays by extracting and using the autofluorescence data which is inherent in the slides.

Since most of this autofluorescence originates in protein molecules, it makes sense that we can use this data as a surrogate for a protein staining dye like eosin. We try to find an optimal transform between the fluorescence and the brightfield images by optimizing transform parameters so that the difference between the virtual and real H&E stain images of the same tissue is minimized.

Since the practical objective of our study is to enable pathologists to annotate the fluorescence images by means of this virtual H&E images generation, we evaluate our transformation by comparing the tumor annotation results done by pathologists on pairs of real and virtual H&E images of the exact same tissue.

The validation of our results shows that the virtual H&E images generated by our algorithm can be used by pathologists for annotation and interpretation purposes and lead to conclusions that are similar to the ones obtained with real H&E images. The similarity can of course also be seen with the naked eye, especially since we have managed to stain and image the exact same tissue sample with both H&E and fluorescence staining. We could potentially use the same technique to also virtually create other brightfield immunohistochemical stains from the fluorescence image data in order to emulate other staining that pathologists feel comfortable working with. The Dice coefficients for the tumor annotation on the test set is above 0.96, demonstrating a high correlation between pathologist annotation of tumor on real H&E slides compared to the tumor annotations on the virtual H&E slides. This high value correlation between annotations on real and virtual slides is precisely what we were trying to achieve since it will enable us to keep staining and imaging tissue with fluorescence technology, enabling multiplexing of many targets simultaneously while still enabling pathologists to diagnose and annotate these images comfortably through the virtualization of brightfield H&E (or other stains) images.

Another interesting question we have yet to address includes whether our transform retains enough high-resolution nuclear details to enable detection of nuclear atypia. In the source, fluorescence images loss of fine grain nuclear details can also originate from saturation of the DAPI staining or the fluorescent imaging system as compared to hematoxylin brightfield imaging. However, as can be seen from Figures 10 and 11, FOVs at ×20 show similar structures on the real and virtual H&E images.

Conclusion

We propose a method for generating virtual brightfield images of H&E stained tissue from fluorescence images of immunohistochemical stained tissue in order to facilitate pathologist annotations of histopathological structures on fluorescence microscopy images. Our method is based on optimizing a transform function using paired slide images stained consecutively with an immunohistochemical fluorescent staining technique and H&E. We validate the results by comparing tumor annotations done by pathologists on real and virtual H&E images. The comparison as well as visual assessment indicate that the virtual stain is similar to the real stain and that pathologists annotations are similar on both real and virtually stained slide images.

Acknowledgment

The authors would like to thank Fabien Gaire, Head of Pathology at Roche Innovation Center Munich, for his support and valuable insights. The authors are grateful to Emilia Anderesson, Konstanty Korksi, Marta Canamero, and Natascha Rieder, the expert pathologist team of Roche, for providing slide annotations and for their helpful comments. The authors gratefully acknowledge the support and cooperation of Sabine

Moosmann and all the lab technicians team. The authors would also like to thank all other members of the pathology department for their support.

Financial support and sponsorship

The research reported in this publication was supported by Roche.

Conflicts of interest

There are no conflicts of interest.

References

1. Fox H. Is H & E morphology coming to an end? Br Med J 2000;9:38-40.
2. Fischer AH, Jacobson KA, Rose J, Zeller R. Hematoxylin and eosin staining of tissue and cell sections. CSH Protoc 2008;3.
3. Haub P, Meckel T. A model based survey of colour deconvolution in diagnostic brightfield microscopy: Error estimation and spectral consideration. Sci Rep 2015;5:12096.
4. Tadrous PJ. Digital stain separation for histological images. J Microsc 2010;240:164-72.
5. Gurcan MN, Boucheron LE, Can A, Madabhushi A, Rajpoot NM, Yener B, *et al.* Histopathological image analysis: A review. IEEE Rev Biomed Eng 2009;2:147-71.
6. Tilli MT, Cabrera MC, Parrish AR, Torre KM, Sidawy MK, Gallagher AL, *et al.* Real-time imaging and characterization of human breast tissue by reflectance confocal microscopy. J Biomed Opt 2007;12:051901.
7. Abeytunge S, Li Y, Larson B, Peterson G, Seltzer E, Toledo-Crow R, *et al.* Confocal microscopy with strip mosaicing for rapid imaging over large areas of excised tissue. J Biomed Opt 2013;18:61227.
8. Schiffhauer LM, Boger JN, Bonfiglio TA, Zavislan JM, Zuley M, Fox CA, *et al.* Confocal microscopy of unfixed breast needle core biopsies: A comparison to fixed and stained sections. BMC Cancer 2009;9:265.
9. Bini J, Spain J, Nehal K, Hazelwood V, DiMarzio C, Rajadhyaksha M, *et al.* Confocal mosaicing microscopy of human skin *ex vivo*: Spectral analysis for digital staining to simulate histology-like appearance. J Biomed Opt 2011;16:076008.
10. Gareau DS. Feasibility of digitally stained multimodal confocal mosaics to simulate histopathology. J Biomed Opt 2009;14:034050.
11. Dobbs J, Krishnamurthy S, Kyrish M, Benveniste AP, Yang W, Richards-Kortum R, *et al.* Confocal fluorescence microscopy for rapid evaluation of invasive tumor cellularity of inflammatory breast carcinoma core needle biopsies. Breast Cancer Res Treat 2015;149:303-10.
12. Giacomelli MG, Husvogt L, Vardeh H, Faulkner-Jones BE, Hornegger J, Connolly JL, *et al.* Virtual hematoxylin and eosin transillumination microscopy using epi-fluorescence imaging. PLoS One 2016;11:e0159337.
13. Can A, Bello O, Gerdes J, Li Q. Inventors System and Methods for Mapping Fluorescent Images into a Bright Field Color Space. US; 2012.
14. Tao YK, Shen D, Sheikine Y, Ahsen OO, Wang HH, Schmolze DB, *et al.* Assessment of breast pathologies using nonlinear microscopy. Proc Natl Acad Sci U S A 2014;111:15304-9.
15. Ruifrok AC, Johnston DA. Quantification of histochemical staining by color deconvolution. Anal Quant Cytol Histol 2001;23:291-9.
16. Yagi Y. Color standardization and optimization in whole slide imaging. Diagn Pathol 2011;6 Suppl 1:S15.
17. Monici M. Cell and tissue autofluorescence research and diagnostic applications. Biotechnol Annu Rev 2005;11:227-56.
18. Dice R. Measures of the amount of ecologic association between species. Ecology 1945;26:297-302.